

## **East India Coastal Current controls the Dissolved Inorganic Carbon in the coastal Bay of Bengal**

**V.V.S.S. Sarma\***, V. R. Kumari, T.N.R. Srinivas, M.S. Krishna, P. Ganapathi, V.S.N. Murty

CSIR-National Institute of Oceanography,  
Regional Centre, 176 Lawsons Bay Colony, Visakhapatnam – 530 017, India

\*Corresponding author (sarmav@nio.org)

### **Abstract**

Monthly variations in dissolved inorganic components (DIC) were measured in the coastal waters off Visakhapatnam in the western Bay of Bengal (BoB) to examine the controlling factors on their distribution and fluxes to the atmosphere. The seasonal variations in the direction of East India Coastal Current (EICC) bring significant variations in the hydrographic properties in the coastal western Bay. Poleward moving EICC from February to May brings in high saline waters to the study region resulting in weak stratification and the coastally trapped upwelling Kelvin Waves aid coastal upwelling. On the other hand, equatorward flowing EICC from October to December brings in low saline, warm waters to the study region resulting in strong stratification, and contributes to lower concentrations of DIC and partial pressure of carbon dioxide ( $p\text{CO}_2$ ) and higher pH. During March - August period, higher concentrations of DIC and  $p\text{CO}_2$  and lower pH were observed due to upwelling of subsurface waters under the influence of an shoreward approaching cyclonic eddy. The DIC, pH and  $p\text{CO}_2$  displayed significant relations with temperature, salinity and chlorophyll-a in the both inshore and offshore region. Biological processes are dominant over mixing effect during March - August in both inshore and offshore regions, while their impact decreases towards offshore. Similarly thermal effect is higher during March-August and salinity effect is significantly higher during October - December when the EICC brings in freshwaters from the northern Bay. It is also noticed that the impact of fluxes variations is significantly low. This study suggests that the physical processes modulate the biological processes significantly to influence the DIC system in the coastal BoB and makes it as a strong source for atmospheric  $\text{CO}_2$  than hitherto hypothesized to be a sink.

## Introduction

The coastal ocean is usually an important sink for atmospheric carbon dioxide (CO<sub>2</sub>) (IGBP, 1993), but the changing environmental conditions due to anthropogenic activities would alter the strength of sink (Bauer et al., 2013; Regnier et al., 2013). Tsunagai et al. (1999) estimated that global coastal ocean absorb about  $\sim 1 \text{ PgC y}^{-1}$  of CO<sub>2</sub>, based on the extrapolation of CO<sub>2</sub> absorption found in the East China Sea to global coastal ocean. In contrast, the coastal oceans in the subtropics, such as northern South China Sea, was found to be a weak source to the atmospheric CO<sub>2</sub> (Zhai et al., 2005, 2013; Dai et al., 2013). These observations revealed that coastal oceans are not always sink for the atmospheric CO<sub>2</sub>. Recent addition of more CO<sub>2</sub> data, and data synthesis activities resulted in decrease in net sink of atmospheric CO<sub>2</sub> by the global coastal ocean to  $\sim 0.2 \text{ PgCy}^{-1}$  (Chen et al., 2013; Laruelle et al., 2014). Despite several efforts to improve realistic estimation of CO<sub>2</sub> absorption (sink) in the global coastal ocean, significant uncertainty still remains due to paucity of data (Borges, 2005; Laruelle et al., 2018).

The Bay of Bengal (BoB), the northeastern part of the Indian Ocean, is a unique region with reference to regional settings (closed on three sides and open to the Indian Ocean in the south), freshwater discharge of variable magnitudes and characteristics (Sarma et al., 2012a) from different rivers such as the Ganges, Godavari, Krishna, Mahanadi (UNESCO, 1979), seasonally reversing coastal currents (Murty et al., 1993; Shetye et al., 1996) and occurrence of seasonal coastal upwelling (Gopalakrishna and Sastry, 1985). Kumar et al. (1996) suggested that coastal BoB acts as a strong sink for atmospheric CO<sub>2</sub> during March/April 1991 and attributed to high biological production driven by nutrients from rivers and a subsequent increase in scavenging of this organic matter to depth by river-borne mineral particles (Ittekkot et al., 1991). In contrast, estuaries are known to be net heterotrophic due to the large inputs of terrestrial organic matter (Green et al., 2006; Dai et al., 2008; Sarma et al., 2009) with supersaturated levels of partial pressure of CO<sub>2</sub> (pCO<sub>2</sub>) by several folds compared to the atmospheric CO<sub>2</sub> (Borges et al., 2005; Chen and Borges, 2009; Laruelle et al., 2010; 2018). Sarma et al. (2012a) report that pCO<sub>2</sub> levels vary between 293 and 15210  $\mu\text{atm}$  in the Indian estuaries opened to the BoB and would in turn enhance pCO<sub>2</sub> levels in the coastal BoB. In contrast, Chen et al. (2012), based on more than 100 estuaries, noticed that super saturation of CO<sub>2</sub> in the upper estuaries, however, the river plumes are significant sink for the atmospheric CO<sub>2</sub>.

Sarma et al. (2012a) measured DIC system for the first time during southwest monsoon (peak discharge period) along the western coastal BoB and observed that northwestern coastal BoB acts as a sink for atmospheric CO<sub>2</sub> due to discharge of relatively alkaline waters by the Ganges river while

southwestern coastal Bay is a source due to discharge of acidic and high pCO<sub>2</sub> waters by peninsular rivers viz., Godavari, Krishna. Therefore, it is suggested that either source or sink of CO<sub>2</sub> in the shelf region depends on the discharged river characteristics. Seasonal reversal of East India Coastal Current (EICC) towards equator during October – December distributes the river-discharge along the coast and brings in large seasonal variations in the water column characteristics along the coastal BoB (Rao et al., 1994; Naqvi et al., 1994; Kumar et al., 1996; Sarma et al., 2013a,b).

The coastal circulation in the western BoB is dominated by the seasonally reversing currents and multiple meso-scale cyclonic and anticyclonic eddies. The seasonal currents constitute a poleward flowing East India Coastal Current (EICC) – also known as the Western Boundary Current (WBC; Shetye et al., 1993; Sanilkumar et al., 1997; Babu et al., 2003; Gangopadhyay et al., 2015). The WBC forms during January and develops best during March-April, and decays by June (Shetye et al., 1993). Sarma et al. (2016) showed that the EICC is dominantly equatorward south of 17°N during November-December 2013, and a poleward coastal current associated with an anticyclonic eddy north of 17°N. Sarma et al. (2015) showed that interannual variability in the observed coastal currents during southwest monsoon (August-September) season is associated with the dynamics of Indian Ocean Dipole (IOD) events of negative IOD in 2010 and positive IOD in 2011. Recent studies based on ADCP current observations and HF (High Frequency) radar surface currents along the east coast of India, the authors (Mukherjee et al., 2014; Mukhopadhyay et al., 2017) report seasonal and intraseasonal variability of EICC. This has motivated us to examine the influence of seasonal EICC on the shelf and nearshore regions off east coast of India on the hydrographic and biogeochemical parameters off Visakhapatnam.

The aim of this study is to examine the factors controlling the DIC system and fluxes of CO<sub>2</sub> to the atmosphere in the coastal BoB through time-series observations of sea water sampling along a transect off Visakhapatnam and also the time series observations of currents at a coastal station north of the above transect using a moored Acoustic Doppler Current Profiler (ADCP) at the depth of 180 m.

## **2. Material and methods**

### *2.1 Study site characteristics*

The continental shelf of east coast of India is relatively narrow, compared to west coast, and it is quite steep in the study region of Visakhapatnam where water column depth of 100 m occurs at ~30 km from the coast (Fig. 1). In the BoB, being a tropical basin, the biological production is modulated to a large extent by physical processes bringing nutrients to the photic layer by seasonal upwelling,

cyclones and heavy rainfall (Maneesha et al., 2011; Sarma et al., 2013a). Though the study region (Fig. 1) does not receive freshwater discharge directly as no rivers are opened within 100 km from north/south of the region, it gets seasonally the low salinity waters of the river in freshwater discharge from the northern Bay through the equatorward flowing EICC during post-monsoon season (October-December). This results in strong salinity stratification during this period (Shetye et al., 1996) and changes the water column characteristics in the study region. In contrast, weak salinity gradient occurs during pre-monsoon season (February-May) due to poleward flowing EICC advecting high-saline waters from south. The mean salinity of the surface waters of the BoB are 2 to 6 lesser due to large freshwater discharge from rivers (Rao et al., 1994) than that of its adjacent basin Arabian Sea.

## *2.2 Sample collection and analysis*

Monthly sea water sampling was conducted on board mechanized boat from 0.5 km from the coast to ~30 km offshore in the coastal BoB, off Visakhapatnam, at six fixed stations along a transect (Fig. 1) at standard depths from January to December 2015. In this study the stations (V1, V2 and V3), occupied within 15 km distance from the coast, are considered as inshore region and the stations (V4, V5 and V6), occupied between 15 and 30 km distance, are considered as offshore region. This classification is done based on the nutrients and Chlorophyll-a (Chl-a) variability between these two regions as per the study of Sarma et al. (2013 a, b). The mean of each parameter for each month at the stations V1-V3 and that of stations V4-V6 are represented as inshore and offshore regions respectively, and are used to construct the annual cycle for inshore and offshore regions. Vertical profiles of pressure, temperature and salinity were measured using a portable conductivity, temperature and depth (CTD) profiler (SBE 19 plus; SeaBird Electronics, US). The water sampling was done at standard depths using 10L Niskin bottle attached to rosette with pressure triggered closing mechanism (ECO rosette sampler, SBE, US). Bubble-free water samples were first collected for dissolved oxygen (DO) followed by dissolved inorganic carbon (DIC), and pH. The DO was measured using Winkler titration method following potentiometric detection (Carpenter, 1966) using potentiometer (Titrand Metrohm, Zofingen, Switzerland). A 2-L water sample was filtered through a GF/F filter (0.7  $\mu\text{m}$  pore size; Whatman) and Chl-a retained on the filter was first extracted with N,N-dimethylformamide (DMF), at 4° C in the dark for 12 h and then spectrofluorometrically analyzed (Varian Eclipse fluorophotometer) following Suzuki and Ishimaru (1990). The analytical precision for Chl-a analysis was  $\pm 0.04 \text{ mg m}^{-3}$ . The concentrations of nutrients were measured following standard spectrophotometric procedures using an auto analyzer (Technicon; Taacs, Australia) (Grasshoff et al. 1983). The detection limits for nitrate, ammonia, phosphate, and silicate

were  $\pm 0.05$ ,  $\pm 0.05$ ,  $\pm 0.02$ , and  $\pm 0.03$   $\mu\text{M}$ , respectively. The pH was measured using glass electrodes (Metrohm, Zofingen, Switzerland) following standard operating procedures suggested by the Department of Energy (DOE, 1998). pH was measured in the NBS scale and then converted to total scale using CO<sub>2</sub>sys program (Lewis and Wallace, 1998). DIC was measured using a coulometer (model CM 5014; UIC Inc., Joliet, IL, USA) attached to an automated subsampling system (Sarma, 1998; 2012a; 2015). The precisions for pH, and DIC were  $\pm 0.002$ , and  $\pm 1.8$   $\mu\text{M}$ , respectively. The accuracy of the pH and DIC was estimated using Certified Reference Material supply by Dr. A.G. Dickson of Scripps Institute of Oceanography, USA as 0.015 and 4  $\mu\text{M}$  respectively. The pCO<sub>2</sub>, calcite and aragonite saturation was computed using the measured salinity, temperature, nutrients (phosphate and silicate), pH and DIC using the CO<sub>2</sub> SYS programme (Lewis and Wallace, 1998) using the CO<sub>2</sub> dissociation constants given by Millero et al. (2006) in the 0-40 salinity range. The accuracy of the estimated pCO<sub>2</sub> is  $\sim 7$   $\mu\text{atm}$ . The air-water flux of CO<sub>2</sub> was estimated using formulations given by Wanninkhof (2014) based on surface pCO<sub>2</sub> levels and monthly mean wind speeds measured close to the study region using automated weather station at 10m above sea level and atmospheric pCO<sub>2</sub> values obtained from CDIAC ([http://cdiac.esd.ornl.gov/pns/current\\_ghg.html](http://cdiac.esd.ornl.gov/pns/current_ghg.html)).

### *2.3 Time-series observations of coastal currents off Visakhapatnam in 2015*

One year long time-series of coastal current measurements were carried out off Visakhapatnam by deploying a mooring fitted with Acoustic Doppler Current Profiler (ADCP, #300kHz; Make: Teledyne RD Instruments, USA) at 180 m at a coastal station (BOVS6: 17°48'N, 83°58'E marked in Fig.1) from 5 March 2015 to 6 March 2016. The ADCP recorded the currents at 4 m depth bins and 30 min interval. Following Mukherjee et al. (2014) and Sarma et al (2015), quality control measures were applied to the ADCP data processing and time-series of currents data were obtained in the depth range of 20-180 m. The processed time-series of zonal (U, east–west flow) and meridional (V, north–south flow) velocity data were 36hr low-pass filtered to remove the tidal and local inertial oscillations (39 hr period) and daily averaged. These data were again subjected to 5-day averages and used in this study. Since there are no data in the top 20 m layer (as per ADCP data acquisition norms and data quality control measures), we have extended the each 5-day averages of U and V values at 20 m depth to the upper 20 m layer for the entire 5-day time-series. Then the depth-integrated zonal and meridional volume transports ( $\text{m}^2 \text{s}^{-1}$  per meter distance) in the 0-100 m layer were computed, following Pond and Pickard (1983). Even if the U and V values are slightly higher or lower than at 20 m depth, the time variation of integrated volume transports do not differ much. In this study, we present the depth-time sections of 5-day averaged zonal and

meridional velocity and the time variation of the depth-integrated zonal and meridional volume transports in the 0-100 m layer for the period of study, i.e. from March 2015 to February 2016.

### 3. Results

#### 3.1. *Monthly variations in hydrographic characteristics in the coastal BoB*

The surface water temperature are cooler ( $<26^{\circ}\text{C}$ ) during winter (January-February), and warmer ( $28^{\circ}$ - $29^{\circ}\text{C}$ ) during March-September, with increased peak value of  $30^{\circ}\text{C}$  in October both in the inshore and offshore regions (Fig. 2). The SST cooling during southwest monsoon was moderate. Water temperatures in the upper 30 m were cooler in the near shore than offshore by  $0.5^{\circ}$ - $2.4^{\circ}\text{C}$  and relatively higher difference was observed between February and September ( $1.1^{\circ}$  to  $2.4^{\circ}\text{C}$ ). Occurrence of strong thermal stratification is present in the upper 30 m between March and August in both inshore and offshore regions. Water column is mostly uniform vertically in the inshore region in winter months whereas a clear thermocline can be observed in the offshore region (Fig. 2). Relatively cooler water was observed between March and August compared to post-monsoon period (October-December). Upsloping of isotherms can be noticed from 40 m depth between March and August in both inshore and offshore regions, and interestingly below 40 m depth dome-like structures are noticed in both temperature and salinity structures from March to August (Figs. 2a-b and Figs. 2c-d). The vertical salinity structures show strong stratification due to freshwater input in the upper 30-40 m during October-December in both inshore and offshore regions. Relatively saltier waters, up to 34.4 to 34.6, were observed in the dome-like structures between March and September.

The Chl-a concentration in the water column ranged from 0.15 to  $4.42\text{ mg m}^{-3}$  in the inshore and  $0.02$  to  $2.48\text{ mg m}^{-3}$  offshore (Figs. 2e-f). More particularly, higher Chl-a ( $>1.0\text{ mg m}^{-3}$ ) was noticeable in the upper 30 m water column from March to September. Maximum Chl-a ( $>4.0\text{ mg m}^{-3}$ ) is associated with low salinity waters in November in the inshore region. In the dome-like structure from May to August, the Chl-a was relatively high in inshore than offshore region. In the offshore region, two peaks in Chl-a were observed in the upper 20-40 m during May-June and November.

#### 3.2 *Monthly variations of currents and volume transport in the coastal BoB*

Figures 3a-c represent the depth-time sections of 5-day averaged zonal and meridional velocity ( $\text{cm s}^{-1}$ ) and the time variation of depth-integrated volume transport ( $\text{m}^2\text{ s}^{-1}$  per unit distance) from March 2015 to February 2016. The HYCOM simulated weekly variations of sea surface height (m) and circulation in June and July 2015 and monthly variations of HYCOM-SSH and circulation for February 2015, May 2015, August 2015 and November 2015 are presented in Figures 4 and 5 respectively. The HYCOM simulated circulation patterns provide spatial variation in the circulation

in the western BoB encompassing the study area. The variations in the observed time-series of currents (Figs. 3a-b) are also used to validate the HYCOM simulated circulation (Figs. 4 and 5). The observed seasonal northeastward flowing EICC in March-April 2015 is seen persisting from February to May 2015 in HYCOM currents (Figs. 4a-b). The EICC attains higher ( $50 \text{ cm s}^{-1}$ ) eastward velocity in March in the 20-160 m depth range and high ( $50 \text{ cm s}^{-1}$ ) northward velocity over a shallow depth range of 20-60 m in April 2015 (Figs. 3a-b). The poleward EICC also attains higher speed at subsurface depths of 100-140 m in March 2015. The poleward flowing EICC exhibits year-to-year variability with its early occurrence in January 2016 and continues to February 2016 with two cores of higher ( $40\text{-}50 \text{ cm s}^{-1}$ ) speeds at 30-70 m and 100-140 m. The poleward EICC flow continues with double core speeds in May and June 2015 and also at subsurface depths in September 2015, highlighting the presence of intraseasonal variability. During the southwest monsoon of 2015, there is a southwestward coastal current with dominant westward flow ( $45\text{-}55 \text{ cm s}^{-1}$ ) at subsurface depths (40-100 m) with two intraseasonal peaks in July. The observed currents during August- early October 2015 show a flow reversal once again to northeastward with strong eastward ( $45 \text{ cm s}^{-1}$ ) and northward ( $35\text{-}45 \text{ cm s}^{-1}$ ) currents with double peaks at deeper depths of 100-160 m (Figs. 3a-b), as also seen in HYCOM simulated circulation in August 2015 (Fig. 4c). This reversal of flow to northeastward during August-early October 2015 is associated with the meso-scale anticyclonic eddy under the impact of the strong positive IOD event (Saji et al., 1999; Subrahmanyam et al., 2011; Sarma et al., 2015). The positive IOD event is associated with positive Dipole Mode Index (DMI) and the negative IOD event with negative DMI, as defined in Saji et al. (1999). In 2015, the DMI of positive IOD is large ( $1^{\circ}\text{-}1.2^{\circ}\text{C}$ ) during July-November 2015 (<http://www.bom.gov.au>). The positive IOD event generates upwelling Kelvin wave in the eastern equatorial Indian Ocean and propagate all along the periphery of coastal BoB and reaches the study region and generates the meso-scale anticyclonic eddy in the western BoB and is well captured by the observed currents and HYCOM simulations. With the weakening of the IOD event, the seasonal EICC is seen flowing equatorward from November with higher speed ( $50 \text{ cm s}^{-1}$ ) in the depth range of 20-80 m and intensifies over a depth range of 20-180 m in December 2015 (Figs. 3a-b), and is well simulated in the HYCOM (Figs. 4d). The observed zonal and meridional currents show a strong current shear with opposing flows at around 80 m in April-June, and around 60 m in July-September (Figs. 3a-b).

The variations of zonal and meridional transports in the upper 100 m layer during March 2015 - February 2016 follow similar pattern (Fig. 3c). The zonal transport is very high and westward in May, July-early August and in December 2015, compared to southward meridional transport in these months. The observed northeastward EICC transport is the highest in March 2015 with its magnitude

reaching to  $40\text{-}50\text{ m}^2\text{ s}^{-1}$  (or  $4\text{-}5 \times 10^6\text{ m}^3\text{ s}^{-1}$  assuming that EICC prevails over  $100\text{ km}$  width). The highest southwestward transport ( $-4.0 \times 10^6\text{ m}^3\text{ s}^{-1}$ ) in July 2015 is due to the southwestward coastal flow associated with the elongated meso-scale cyclonic eddy encompassing the study region and its westward movement. This can be clearly seen in the HYCOM simulated weekly currents in June to July (Figs. 5a-d). The northeastward transport ( $\sim 2.0 \times 10^6\text{ m}^3\text{ s}^{-1}$ ) weakens in August-September 2015 due to weakening of the cyclonic eddy flow (Fig. 4c). The higher magnitude of southwestward transport ( $5\text{-}6 \times 10^6\text{ m}^3\text{ s}^{-1}$ ) during November 2015-early January 2016 is associated with the equatorward flowing EICC. Once again, there is a quick reversal of EICC to flow southwestward in February 2016 with higher southwestward transport of  $4\text{-}5 \times 10^6\text{ m}^3\text{ s}^{-1}$  under the impact of the development of negative IOD ( $-0.5^\circ\text{C}$ ) by January 2016. This is in agreement with the studies of Subrahmanyam et al. (2011) and Sarma et al. (2015).

### 3.3. Monthly variations in dissolved inorganic carbon components in the coastal BoB

The monthly variations in DIC, pH and  $\text{pCO}_2$  resemble those of temperature, salinity and Chl-a in the coastal BoB (Fig. 6). The concentrations of DIC varied between  $1700$  and  $2140\text{ }\mu\text{M}$  with the lower concentrations in the upper  $30\text{ m}$  in November associated with low salinity waters in the inshore and also offshore regions (Fig. 2) brought in by the southwestward flowing EICC (Figs. 3a-c and Fig. 4d). Higher concentrations of DIC ( $>2000\text{ }\mu\text{M}$ ) were observed from March to September in association with the doming of isolines from  $100\text{ m}$  to  $10\text{ m}$  depth in the inshore and offshore regions. The pH varied between  $8.03$  and  $8.22$  and higher pH was observed in November in association with the equatorward EICC flow of low salinity waters. Lower pH during March-September coincides with the occurrence of higher salinity and lower temperature (Fig. 2 and Fig. 5). The  $\text{pCO}_2$  in the surface waters ranged between  $320$  and  $650\text{ }\mu\text{atm}$  with higher levels from March to August and under-saturation levels from October to December (Fig. 6). Both calcite and aragonite were above the saturation level during entire study period, however, the saturation level was relatively low during March-September than other months. The highest saturation of calcite and aragonite was observed during November and December (Fig. 6). The surface  $\text{pCO}_2$  levels were relatively higher in the inshore than offshore regions. The sea-to-air fluxes of  $\text{CO}_2$  varied from  $-0.77$  to  $3.18\text{ mmolCm}^{-2}\text{d}^{-1}$  in the inshore region and  $-1.47$  to  $0.78\text{ mmolC m}^{-2}\text{d}^{-1}$  in the offshore region and relatively higher fluxes to atmosphere were observed during March-August (Fig. 6).

The DIC displayed significant linear relation with salinity ( $r^2=0.88$ ;  $p>0.001$ ) and inverse relation with temperature ( $r^2=0.34$ ;  $p<0.01$ ) in the study region (Fig. 7). DIC also displayed significant inverse relation with Chl-a in the inshore waters ( $r^2=0.52$ ;  $p<0.001$ ) and weak relation in the offshore



waters ( $r^2=0.28$ ;  $p<0.05$ ). Similarly the  $p\text{CO}_2$  also displayed significant relation with salinity ( $r^2=0.61$ ;  $p<0.001$ ), and weaker relations with temperature ( $r^2=0.31$ ;  $p<0.05$ ) and Chl-a ( $r^2=0.25$ ;  $p<0.05$ ) (Fig. 7). The relation of salinity with DIC and total alkalinity, computed from DIC and pH, was plotted with linear mixing line (Fig. 8). The data collected between October and January were found to fall below the mixing line whereas the data at the higher salinity, during March to August, fallen above the mixing line.

#### 4. Discussion

##### 4.1. Influence of coastal circulation on hydrographic characteristics of coastal BoB

The spatial variations in temperature and salinity depend on the coastal currents and also on the input of freshwater from the land. The northwestern coastal Bay receives enormous amount of freshwater from the Ganges river ( $>14000 \text{ m}^3\text{s}^{-1}$ ; Sarma et al., 2012a) than peninsular rivers in the south ( $<1000 \text{ m}^3\text{s}^{-1}$ ; Krishna et al., 2015). This results in cooler temperature and higher salinity in the south due to weak stratification and *vice versa* in the north. The temperature and salinity variations in the study region are mainly driven by seasonal variations in EICC. The EICC flow is poleward during February-May and brings high saline waters from the south to the study region. As a result, the vertical stratification weakens resulting in occurrence of vertical mixing. The doming of isotherms and isohalines during March-August 2015 is due to westward movement of cyclonic eddy from open Bay (Figs. 4a-c or Figs. 5a-d) as seen in the HYCOM simulated Sea Surface Height and circulation) and aids upwelling of subsurface waters. This brings cooler, high saline and nutrient rich waters to the surface. Enhancement of nutrients concentrations to surface by 1.5 to 2 times was observed due to upwelling associated with the divergence of waters in the cyclonic eddy. As a result of increased nutrient concentrations, phytoplankton biomass (Chl-a) increased from lower concentrations ( $0.25\text{-}0.5 \text{ mg m}^{-3}$ ) in January-February to higher concentrations ( $1\text{-}4 \text{ mg m}^{-3}$ ) in March-August in the inshore region and the corresponding values are less ( $0.04\text{-}0.25$  to  $0.3\text{-}1.7 \text{ mgm}^{-3}$ ) in the offshore region(Fig. 2), which are consistent with the temperature and salinity structures.

Sarma et al. (2012a) noticed very low saline waters in the northwestern Bay during July-August in association with higher river discharge containing relatively low nutrients and suspended load and high phytoplankton biomass due to deeper photic depth. Contrasting conditions were observed in the southwestern coastal Bay during July-August (Sarma et al., 2013b; Bandopadhyay et al., 2017). The direction of EICC flow reverses equatorward during September-December (Fig. 4d) and brings fresh waters from northern Bay to the study region (Shetye et al., 1996; Varkey et al., 1996). The entire water column of the inshore waters is filled with low saline waters, while strong stratification occurs

in the offshore region with freshwater lens in the upper 30-40 m. Advection of the low saline waters of the northern Bay to the study region by the equatorward EICC in November modified the hydrographic conditions in the study region (Fig. 3 and Figs. 4d). Therefore, the variations in the coastal hydrography are controlled by seasonally reversing EICC and it has a significant impact on DIC components.

#### 4.2. Influence of coastal circulation on dissolved inorganic carbon system in the coastal BoB

Concentrations of DIC showed significant intra-annual variability associated with physical processes- salinity stratification, seasonal reversal flow of EICC, cyclonic eddy and coastal upwelling. Relatively higher DIC was observed during March-August associated with the shoreward movement of a cyclonic eddy from the open Bay (Figs. 4b-c and Figs. 5a-d) with a peak divergence of cold, nutrient rich subsurface waters to the euphotic layer in June. The impact of divergence and the upwelling was observed in both inshore region and offshore region. The mean DIC during March-August was high (between 2030  $\mu\text{M}$  and  $\sim 2115 \mu\text{M}$ ) in the inshore and offshore regions (Fig. 6). The seasonal reversal of EICC from October to December brought low salinity and low DIC waters from the northern Bay (Kumar et al., 1996; Sarma et al., 2012b) and the DIC concentrations decreased significantly during this period in the study region. The pH also displayed similar distribution pattern with relatively lower pH during March-August and higher pH during October-December (Fig. 6). Advection of basic waters from the northern Bay by the equatorward EICC increased the pH in the study region during October-December. This is further confirmed by occurrence of low saline waters (by  $\sim 10$  psu) during October-December. The pH in the Ganges estuary was higher ( $8.130 \pm 0.24$ ) compared to the peninsular river estuaries (7.020 to 7.470; Sarma et al., 2012a; Mukhopadhyay et al., 2002). The  $\text{pCO}_2$  concentrations were relatively higher, above atmospheric value, during March-August ( $>550 \mu\text{atm}$ ) and then decreased significantly to under-saturation concentrations ( $<400 \mu\text{atm}$ ) with reference to the atmospheric value during October-December (Fig. 6). Perennial occurrence of low  $\text{pCO}_2$  levels, below atmospheric value, was reported in the northern Bay (Kumar et al., 1996; Sarma et al., 2012a) due to freshwater input from the Ganges river. The  $\text{pCO}_2$  levels in the Ganges river were about  $502 \pm 100 \mu\text{atm}$  which is an order of magnitude less than that of peninsular river estuaries (4981-17205  $\mu\text{atm}$ ; Sarma et al., 2012a). The equatorward advection of low salinity and low  $\text{pCO}_2$  waters by the EICC from the northwestern Bay decreased the  $\text{pCO}_2$  concentrations during October-December in the study region. Both aragonite and calcite were above saturation during entire study period and relatively low saturation values were observed during March to September associated with coastal upwelling and injection of low pH waters from subsurface (Fig. 6). The aragonite saturation below 30 m depth in the open sea region

was close to saturation (<2%) whereas freshwater discharge enhanced saturation levels to the maximum during November and December (Fig. 6).

In order to differentiate the dominance of physical versus biological processes, DIC was normalized to constant salinity following Friis et al.(2003) and correlated with Chl-a ( $r^2=0.44$ ;  $p<0.001$ ) and dissolved oxygen saturation ( $r^2=0.32$ ;  $p<0.001$ ), which are a measure of biological processes. These relationships suggest that both biological and physical processes are important in controlling DIC concentrations in the coastal BoB. Significant correlation of DIC with Chl-a cannot be expected as DIC is also modified by heterotrophic activity and also Chl-a is not a measure of primary production as several other factors such as light, mixing, and grazing also determine primary production. On the other hand strong linear relation of DIC with DO saturation suggests that dominant autotrophy controls variations in DIC in the study region. The mean surface water DO was relatively saturated by 3-4% in the inshore and 1-2% in the offshore region associated with high DIC during March-August suggesting that dominant autotrophy in the coastal BoB. The pH showed significant linear inverse correlation with salinity ( $r^2 = 0.51$ ;  $p<0.001$ ) suggesting that advection of low saline coastal waters contained relatively basic pH, which were influenced by river discharge from Ganges river (Fig. 7). The pH also displayed significant linear relation with temperature ( $r^2 = 0.65$ ;  $p<0.001$ ) suggesting that mixing with deeper waters decreased pH in the study region. Significant linear relation was observed between salinity with DIC and  $pCO_2$  and inverse relation with temperature suggesting vertical mixing and advection of low salinity controls the DIC and  $pCO_2$  levels in the study region. The  $pCO_2$  also displayed inverse weak relation with Chl-a suggesting a significant removal through biological processes (Fig. 7). The relationships of DIC components with physical and biological variables suggest that significant role of physical and associated biological processes may be controlling their variability in the coastal BoB. Both DIC and TA were plotted with salinity with linear mixing line in Figure 8. The end member data in the Indian rivers and open ocean were taken from literature (Sarma et al., 2012b; Prasad et al., 2013 and our unpublished data). The linear relation of salinity with DIC, for the data collected between October and January, is extrapolated to the zero salinity yielded intercept of 742  $\mu M$  (red line) whereas the freshwater end member is  $1000 \pm 22 \mu M$  (Fig. 8) and the difference of these two indicates that biological removal is a dominant mechanism controlling inorganic carbon system. Similarly, salinity and TA relationship yielded intercept of 935  $\mu M$  which is smaller than freshwater end member of 1250  $\mu M$  (Fig. 8). Both DIC and TA values are above the mixing line during March to August suggesting that respiration, and carbonate dissolution may be dominant factors in controlling their distribution (Fig. 8).

### 4.3. Controls of dissolved inorganic carbon in the coastal BoB

In order to quantify the role of physical and biological processes on variations in  $p\text{CO}_2$  in the coastal BoB, the contribution of different effects on  $p\text{CO}_2$  was estimated following the model study of Louanchi et al. (1996). Based on the monthly variations in characteristics of inorganic carbon, the contribution of changes in  $p\text{CO}_2$  due to biological process (primary production and respiration constitute the biological effect), mixing with subsurface waters (mixing effect), variations in temperature and salinity resulted from changes in solubility (thermal effect) and variations in fluxes at sea-air interface (flux effect) were evaluated and presented in Figure 9. The biological effect is computed based on the monthly variations in phytoplankton biomass (Chl-*a*) and dissolved inorganic nitrate. In this model, about 50% of the production is assumed to be respired and 20% of the production is assumed to be exported to the deeper layers. These assumptions are reasonable based on the in situ data in the northern Indian Ocean (Buesseler et al., 1998; Honjo et al., 1999; Kumar et al., 2004; Sherin et al., 2018). The mixing effect is computed based on the variations in the depth of mixed layer and gradient in DIC between below and above the mixed layer. Thermal effect is computed based on the monthly variations in temperature and salinity following Goyet et al. (1993). This analysis suggested that biological effect and mixing effect were the dominant controlling factors followed by thermal and flux effects. Both biological and thermal effects (except January-February and August-September) decreased  $p\text{CO}_2$  by 29 to 179 and -88 to 67  $\mu\text{atm}$  respectively whereas mixing increased  $p\text{CO}_2$  by 2 to 121  $\mu\text{atm}$  in the inshore region of the coastal BoB. On the other hand, the biological, thermal and mixing effects were relatively lower (-24 to -102  $\mu\text{atm}$ , -74 to 58  $\mu\text{atm}$  and 2 to 63  $\mu\text{atm}$  respectively) in the offshore compared to inshore waters, but the direction of variability is same. On the other hand, the contribution of flux effect in variations in  $p\text{CO}_2$  was relatively low due to weak winds, but it changed  $p\text{CO}_2$  by 0.4 to 10.6  $\mu\text{atm}$  in both the regions. The biological effect was low during January-February in the inshore ( $\sim 30 \mu\text{atm}$ ) and offshore waters ( $\sim 25 \mu\text{atm}$ ) and its impact rapidly increased to 50-179 in the inshore region and 41-102  $\mu\text{atm}$  in the offshore region respectively due to divergence associated under the influence of cyclonic eddy during March-August and decreased further after the weakened cyclonic eddy (132-169  $\mu\text{atm}$  in the inshore region and 48-90  $\mu\text{atm}$  in the inshore region). Similarly, the mixing effect contributed significantly during the cyclonic eddy (March-August) in the inshore (36-121  $\mu\text{atm}$ ) and offshore (2-63  $\mu\text{atm}$ ) region with minimal effect during October-December associated with strong salinity stratification (Fig. 2). The effect of biology dominated over mixing effect during March-August in both inshore and offshore regions. Thermal effect enhanced  $p\text{CO}_2$  levels during January-March in the inshore (6-67  $\mu\text{atm}$ ) and offshore regions (16-58  $\mu\text{atm}$ ) and this effect decreased  $p\text{CO}_2$  levels in the

inshore (13-28 $\mu$ atm) and offshore (13-23 $\mu$ atm) during March-August. The advection of low salinity waters during October-December decreased pCO<sub>2</sub> by 57-88  $\mu$ atm in the inshore waters and 29-64  $\mu$ atm in the offshore waters due to increase in solubility (Fig. 6). In order to understand the net effect of these processes on pCO<sub>2</sub>, the processes decreasing the pCO<sub>2</sub> were summed and compared with the processes that increased the pCO<sub>2</sub> levels. It suggested that biological effect was dominant during July-December and mixing affect is significant during January - March and all influencing processes were close to balance during April and June. Sarma et al. (2000) noticed that mixing effect is the dominant among others during northeast (winter) and southwest (summer) monsoon in the Arabian Sea due to convective mixing and upwelling respectively. In contrast, biological effect dominated over half of the year followed by mixing effect in the BoB suggesting that biology responses rapidly in the BoB than Arabian Sea due to shallow nitracline depth in the former than latter basin (Rao et al., 1994). In addition salinity impact is significant during October-November, which is contributed by change in direction of EICC. Despite dominant biological effect over mixing during June to December, pCO<sub>2</sub> levels were higher than atmospheric values during June to September (Fig. 6) suggesting that enhanced bacterial respiration may be possible. Fernandes et al. (2008) observed enhanced bacterial abundance and respiration rates associated with freshwater discharge. Therefore, the in situ microbial decomposition rates may be above the modelled values of 50% of primary production. Bacterial respiration rates with reference to freshwater discharge in the coastal BoB are unknown and it is highly essential to evaluate its impact on pCO<sub>2</sub> levels in the coastal BoB.

#### 4.4. Fluxes of CO<sub>2</sub> to the atmosphere

The sea-to-air fluxes of CO<sub>2</sub> were relatively lower in the inshore (-0.77 to 3.18 mmolC m<sup>-2</sup> d<sup>-1</sup>) than offshore (-1.47 to 0.78 mmolC m<sup>-2</sup> d<sup>-1</sup>) due to low pCO<sub>2</sub> levels in the latter region. The CO<sub>2</sub> flux was high and acts as a source to the atmosphere during March-August (westward movement of cyclonic eddy) and it is a sink during other period (October – December) in both inshore and offshore regions. The monthly mean wind speed varied narrowly between 1.0 and 2.6 m/s with no significant monthly variability suggesting that the variability in the flux is driven by variability in pCO<sub>2</sub> levels which in turn controlled by variations in the coastal circulation. On annual basis, the study region acted as a strong source to the atmospheric CO<sub>2</sub> by ~10 times in the inshore (395.8 mmolC m<sup>-2</sup> y<sup>-1</sup>) than offshore (43.6 mmolC m<sup>-2</sup> y<sup>-1</sup>) region in the coastal BoB than hitherto hypothesized as a sink for atmospheric CO<sub>2</sub> (Kumar et al., 1996).

## 5. Summary and Conclusion

Temporal variability in the dissolved inorganic carbon components were measured using monthly time-series observations in the coastal western BoB in the inshore and offshore regions. Seasonal reversal in the direction of EICC regulated the hydrographic characteristics with relatively high saline and low temperature subsurface waters of weak stratification due to cyclonic eddy during March-August, and contrasting to that was observed during October-December period, of equatorward flow of EICC. The westward movement of cyclonic eddy and the associated divergence of cold and saline waters from subsurface depths to euphotic zone during March -August leads to increase of DIC, pCO<sub>2</sub> and decrease in pH of coastal waters. The pCO<sub>2</sub> levels due to cyclonic eddy were 1.5 times higher than the atmospheric value. On the other hand, strong stratification due to advection of low salinity waters during October - December led to low DIC and pCO<sub>2</sub>, which is significantly lower than that of atmospheric CO<sub>2</sub> value. The variability in pCO<sub>2</sub> is mainly controlled by biological processes followed by mixing and thermal (including salinity) effect. The contribution of flux variations was relatively minimal due to weak winds. The coastal BoB acted as a strong source for the atmospheric CO<sub>2</sub> during March-August while sink during October-December period in both inshore and offshore region. The annual mean fluxes of CO<sub>2</sub> in the inshore region acted as a strong source for the atmospheric CO<sub>2</sub> by ~10 times than offshore region. This study suggested that coastal BoB is a strong source to the atmospheric CO<sub>2</sub> than hitherto hypothesized as sink.

Acknowledgements: We would like to thank Director, CSIR-National Institute of Oceanography for this constant encouragement and support. We would like to thank Dr. Dileep Kumar, former DU leader, who supported to set up this time-series observations. We would appreciate the help tendered by boat personnel and project staff during sampling. This has NIO contribution number.....

## References

- Babu, M. T, Sarma, Y. V. B., Murty, V. S. N. and Vethamony, P., 2003. On the circulation in the BoB during Northern spring inter-monsoon (March-April 1987). *Deep Sea Res. Part II*. **50**, 855-865.
- Bandyopadhyay, D., Biswas, H. and Sarma, V. V. S. S., 2017. Impacts of SW Monsoon on Phytoplankton Community Structure along the Western Coastal BOB: an HPLC Approach. *Estuaries and Coasts*. **40**, 1066–1081. DOI 10.1007/s12237-016-0198-6.
- Bauer, J. E., Cai, W.-J., Raymond, P. A., Bianchi, T. S., Hopkinson, C. S., and Regnier, P. A. G., 2013. The changing carbon cycle of the coastal ocean. *Nature*. **504**, 61–70.

- Borges, A.V., 2005. Do we have enough pieces of the jigsaw to integrate CO<sub>2</sub> fluxes in the coastal ocean. *Estuaries*. **28**, 3-27.
- Borges, A. V., Delille, B. and Frankignoulle, M., 2005. Budgeting sinks and sources of CO<sub>2</sub> in the coastal ocean: diversity of ecosystems counts. *Geophys. Res. Lett.* **32**, L14601.
- Buesseler, K., Ball, L., Andrews, J., Beniteznelson, C., Belostock, R., Chai, F., and Chao, Y. 1998. Upper ocean export of particulate organic carbon in the Arabian Sea derived from thorium-234, *Deep Sea Res., Part II*, **45**, 2461–2488.
- Carpenter, J.H., 1966. New measurements of oxygen solubility in pure and natural waters. *Limnology and Oceanography*. **11**, 264-277.
- Chen, C. T. A. and Borges, A. V., 2009. Reconciling opposing views on carbon cycling in the coastal ocean: continental shelves as sinks and near-shore ecosystems as sources of atmospheric CO<sub>2</sub>. *Deep-Sea Res. Part II*. **56**, 578-590, doi: 10.1016/j.dsr2.2009.01.001.
- Chen, C.T.A., Huang, T.H., Fu, Y.H., Bai, Y. and He, X. 2012. Strong sources of CO<sub>2</sub> in upper estuaries become sinks of CO<sub>2</sub> in large river plumes. *Curr. Opin. Environ. Sustain.* **4**, 179-185.
- Chen, C.T. A., Huang, T.-H., Chen, Y.-C., Bai, Y., He, X., and Kang, Y., 2013. Air-sea exchanges of CO<sub>2</sub> in the world's coastal seas. *Biogeosciences*. **10**, 6509–6544, doi:10.5194/bg-10-6509.
- Dai, M., Zhai, W., Cai, W. J., Callahan, J., Huang, B. and coauthors., 2008. Effects of an estuarine plume-associated bloom on the carbonate system in the lower reaches of the Pearl River estuary and the coastal zone of the northern South China Sea. *Cont. Shelf Res.* **28**, 1416-1423.
- Dai, M., Cao, Z, Guo, X., Zhai, W., Liu, Z., Yin, Z., Xu, Y., Gan, J., Hu, J., Chuanjun, D. 2013. Why are some marginal seas sources of atmospheric CO<sub>2</sub>?. *Geophys. Res Lettrs.* **40**. 2154-2158. 10.1002/grl.50390.
- DOE (Department of Energy)., 1998. Determination of total alkalinity in sea water. In: *Hand Book of Methods for the Analysis of the Various Parameters of the Carbon Dioxide System in Seawater*. Version 2 (eds. A. G. Dickson and C. Goyet). Carbon Dioxide Information and Analysis Center, Oak Ridge, TN, ORNL/CDIAC-74, pp. 56-85.
- Doney, S.C., Mahowald, N., Lima, I., Feely, R.A., Mackenzie, F.T., et al., 2007. Impact of anthropogenic atmospheric nitrogen and sulfur deposition on ocean acidification and the inorganic carbon system. *Proc. Natl. Acad. Sci. USA*. **104**, 14580-14585. doi: 10.1073/pnas.0702218104.
- Fernandes, V., Ramaiah, N., Paul, J.T., Sardesai, S., Jyoti Babu, R., Gauns, M. 2008. Strong variability in bacterioplankton abundance and production in central and western Bay of Bengal, *Mar. Biol.* **153**, 975-985.

- Friis, K., Körtzinger, A. and Wallace, D.W.R., 2003. The salinity normalization of marine inorganic carbon chemistry data. *Geophys. Res. Lett.* **30** (2), 1085. doi:10.1029/2002GL015898.
- Gangopadhyay, A., Bharatraj, G.N., Chaudhuri, A.H., Babu, M.T., Sengupta, D., 2013. On the nature of meandering of the springtime western boundary current in the Bay of Bengal. *Geophys. Res. Lett.* **40**, 2188–2193. doi:10.1002/grl.50412.
- Gopalakrishna, V.V. and J.S. Sastry, J.S., 1985. Surface circulation over the shelf off the east coast of India during the southwest monsoon. *Indian J. Mar.Sci.* **14**, 62-65.
- Goyet, C., Millero, F.J., Poisson, A. and Shafer, D.K., 1993. Temperature dependence of CO<sub>2</sub> fugacity in seawater. *Mar. Chem.*, 44: 205-219.
- Grasshoff K, Ehrhardt M and Kremling K (eds) 1983. *Methods of Seawater Analysis*; Weinheim: *Verlag Chemie*, pp. 89–224.
- Green, R. E., Bianchi, T. S., Dagg, M. J., Walker, N. D. and Breed, G. A., 2006. An organic carbon budget for the Mississippi River turbidity plume and plume contributions to air-sea CO<sub>2</sub> fluxes and bottom water hypoxia. *Estuaries and Coasts.* **29**, 579-597.
- Honjo, S., Dymond, J., Prell, W. and Ittekkot, V. 1999. Monsoon-controlled export fluxes to the interior of the Arabian Sea, *DeepSea Res., Part II*, **46**, 1859–1902.
- International Geosphere Biosphere Program (IGBP)., 1993. *Land-Ocean Interactions in the Coastal Zone*, Science Plan. IGBP of ICSU, Reportno. 25, Stockholm, 50 pp.
- Ittekkot, V., Nair, R. R., Honjo, S., Ramaswamy, V., Bartsch, M. and co-authors., 1991. Enhanced particle fluxes in Bay of Bengal induced by injection of fresh water. *Nature.* **351**, 385-387.
- Kumar, M.D., Naqvi, S.W.A., George, M.D., Jayakumar, D.A., 1996. A sink for atmospheric carbon dioxide in the northeast Indian Ocean. *J. Geophys. Res.* **101**, 18121-18125.
- Kumar, S., Ramesh, R., Sardesai, S., Sheshshayee, M.S., 2004. High new production in the Bay of Bengal: possible causes and implications. *Geophys. Res. Lett.* **31**, L18304.
- Krishna, M.S., Prasad, V.R., Sarma, V.V.S.S., Reddy, N.P.C., Hemalatha, K.P.J., Rao, Y.V., 2015. Fluxes of dissolved organic carbon and nitrogen to the northern Indian Ocean from the Indian monsoonal rivers. *J. Geophys. Res. Biogeoscience.* **120**(10), 2067-2080.
- Laruelle, G. G., Durr, H. H., Slomp, C. P. and Borges, A. V., 2010. Evaluation of sinks and sources of CO<sub>2</sub> in the global coastal ocean using a spatially-explicit typology of estuaries and continental shelves. *Geophys. Res. Lett.* **37**, L15607.
- Laruelle, G. G., Lauerwald, R., Pfeil, B., and Regnier, P., 2014. Regionalized global budget of the CO<sub>2</sub> exchange at the air-water interface in continental shelf seas. *Global Biogeochem. Cy.* **28**, 1199–1214, doi:10.1002/2014GB004832.



- Laruelle, G.G., Cai, W.J., Hu, X., Gruber, N., Mackenzie, F.T., and Regnier, P. 2018. Continental shelves as a variable but increasing global sink for atmospheric carbon dioxide, *Nature Commun.* **9**, 454.
- Lewis, E., Wallace, D. W. R., 1998. Program Developed for CO<sub>2</sub> System Calculations. Carbon Dioxide Information Analysis Center, Oak Ridge National Laboratory, U.S. Department of Energy, Oak Ridge, TN. ORNL/CDIAC-105.
- Louanchi, F., Metzl, N., and Poisson, A., 1996. Modelling the monthly sea surface pCO<sub>2</sub> fields in the Indian Ocean. *Mar. Chem.* **55**, 265–279.
- Maneesha, K., Sarma, V.V.S.S., Reddy, N.P.C., Sadhuram, Y., Murty, T.V.R., Sarma, V.V. and Dileep Kumar, M., 2011. Meso-scale atmospheric events promote phytoplankton blooms in the coastal Bay of Bengal. *J. Earth Sys. Sci.* **120**(4), 773–782.
- Millero, F. J., Graham, T. B., Huang, F., Bustos-Serrano, H., Perrot, D., 2006. Dissociation constants of carbonic acid in seawater as a function of salinity and temperature. *Mar. Chem.* **100**, 80-94.
- Mukherjee, A., Shankar, D., Fernando, V., Amol, P., Aparna, S.G., Fernandes, R., Michael, G.S., Khalap, S. T., Satelkar, N. P., Agarvadekar, Y., Gaonkar, M. G., Tari, A. P., Kankonkar, A. and Vernekar, S., 2014. Observed seasonal and intraseasonal variability of the East India Coastal Current on the continental slope. *J. Earth Syst. Sci.* **123**, 1197. <https://doi.org/10.1007/s12040-014-0471-7>.
- Mukhopadhyay, S. K., Biswas, H., De, T. K., Sen, S. and Jana, T. K., 2002. Seasonal effects on the air-water carbon dioxide exchange in the Hooghly estuary, NE coast of Bay of Bengal, India. *J. Environ. Monit.* **4**, 549-552.
- Mukhopadhyay, S., Shankar, D., Aparna, S.G. and Mukherjee. A., 2017. Observations of the sub-inertial, near-surface East India Coastal Current. *Cont. Shelf Res.* **148**, 159-177. <https://doi.org/10.1016/j.csr.2017.08.020>
- Murty, C. S. and Varadachari, V. V. R., 1968. Upwelling along the east coast of India. *Bull. Natl. Inst. Sci. India.* **36**, 80-86.
- Murty, V. S. N., Suryanarayana, A. and Rao. D. P., 1993. Current structure and volume transport across 12°N in the Bay of Bengal. *Indian J. Mar. Sci.* **22**, 12–16.
- Naqvi, S. W. A., Jayakumar, D. A., Nair, M., Kumar, M. D. and George, M. D., 1994. Nitrous oxide in the western Bay of Bengal. *Mar. Chem.* **47**, 269-278.
- Pond, S. and Pickard, G.L., 1983. *Introductory Dynamical Oceanography*. 2<sup>nd</sup> Edition, Pergamon Press, Oxford.
- Prasad, M.H.K., Sarma, V.V.S.S., Sarma, V.V., Krishna, M.S. and Reddy, N.P.C. 2013.

Carbon dioxide emissions from the tropical Dowleiswaram reservoir on the Godavari

River, southeast of India, *J Water Resource and Prot.*, **5**, 534-545.

Rao, C. K., Naqvi, S. W. A., Kumar, M. D., Varaprasad, S. J. D., Jayakumar, D. A. and co-authors., 1994. Hydrochemistry of the Bay of Bengal: possible reasons for a different water-column cycling of carbon and nitrogen from the Arabian Sea. *Mar. Chem.* **47**, 279-290.

Regnier, P., Friedlingstein, P., Ciais, P., Mackenzie, F. T., Gruber, N., Janssens, I., Laruelle, G. G., Lauerwald, R., Luysaert, S., Andersson, A. J., Arndt, S., Arnosti, C., Borges, A. V., Dale, A. W., Gallego-Sala, A., Godd ris, Y., Goossens, N., Hartmann, J., Heinze, C., Ilyina, T., Joos, F., LaRowe, D. E., Leifeld, J., Meysman, F. J. R., Munhoven, G., Raymond, P. A., Spahni, R., Suntharalingam, P. and Thullner, M., 2013. Anthropogenic perturbation of the carbon fluxes from land to ocean. *Nat. Geosci.* **6**, 597–607, doi:10.1038/ngeo1830.

Sanilkumar, K.V., Kuruvilla, T.V., Jogendranath, D. and Rao, R.R., 1997. Observations of the Western Boundary Current of the Bay of Bengal from a hydrographic survey during March 1993. *Deep-Sea Res. I*, **44** (1), 135-145.

Saji, N. H., Goswami, B. N., Vinayachandran, P. N., & Yamagata, T. (1999), A dipole mode in the tropical Indian Ocean. *Nature*, **401**(6751), 360.

Sarma, V. V. S. S., 1998. Variability in Forms and Fluxes of Carbon Dioxide in the Arabian Sea. PhD Thesis. Goa University, Goa, India, pp. 1-256 (*unpublished*)

Sarma, V. V. S. S., Kumar, M. D., Gauns, M., and Madhupratap, M., 2000. Seasonal controls on surface pCO<sub>2</sub> in the central and eastern Arabian Sea. *Proc. Indian Acad. Sci. (Earth Planet. Sci.)*, **109**, 471–479.

Sarma, V. V. S. S., Gupta, S. N. M., Babu, P. V. R., Acharya, T., Harikrishnachari, N. and co-authors., 2009. Influence of river discharge on plankton metabolic rates in the tropical monsoon driven Godavari estuary, India. *Eastur. Coastal Shelf Sci.* **85**, 515-524.

Sarma, V. V. S. S., Krishna, M. S., Rao, V. D., Viswanadham, R., Kumar, N. A., Kumai, V. R et al., 2012a. Sources and Sinks of CO<sub>2</sub> in the west coast of Bay of Bengal. *Tellus B.* **64**, 10961, doi: 3402/tellusb.v64i0.10961.

Sarma, V. V. S. S., Viswanadham, R., Rao, G. D., Kumar, B. S. K., Prasad, V. R., Naidu, S. A., et al., 2012b. Carbon dioxide emissions from Indian monsoonal Estuaries. *Geophys. Res. Lett.* **39**, doi:10.1029/2011GL050709.

Sarma, V.V.S.S., Krishna, M.S., Viswanadham, R., Rao, G.D., Rao, V.D., Sridevi, B., Kumar, B.S.K., Prasad, V.R., Subbaiah, Ch.V., Acharyya, T. and Bandopadhyay, D., 2013b. Intensified oxygen minimum zone on the western shelf of BOB during summer monsoon: influence of river discharge. *J. Oceanogr.* **69**(1), 45–55.

Sarma, V.V.S.S., Sridevi, B., Maneesha, K., Sridevi, T., Naidu, S.A., Prasad, V.R., Venkataramana, V., Acharya, T., Bharati, M.D., Subbaiah, C.V., Kiran, B.S., Reddy, N.P.C., Sarma, V.V., Sadhuram, Y., Murty, T.V.R., 2013a. Impact of atmospheric and physical forcings on

- biogeochemical cycling of dissolved oxygen and nutrients in the coastal Bay of Bengal. *J. Oceanogr.* **69**(2), 229-243.
- Sarma, V. V. S. S., Krishna, M. S., Paul, Y. S. and Murthy, V. S. N., 2015. Observed changes in ocean acidity and carbon dioxide exchange in the coastal Bay of Bengal - a link to air pollution. *Tellus B.* **67**, 24638.
- Sarma, V.V.S.S., G.D. Rao, R. Viswanadham, C.K. Sherin, J. Salisbury, M.M. Omand, A. Mahadevan, V.S.N. Murty, E.L. Shroyer, M. Baumgartner, K.Stafford., 2016. Effects of freshwater stratification on nutrients, dissolved oxygen and phytoplankton in the Bay of Bengal. *Oceanogra.*, **29**, 126-135.
- Sherin, C.K., Sarma, V.V.S.S., Rao, G.D., Viswanadham, R., Omand, M.M., and Murty, V.S.N. 2018. New to total primary production ratio (f-ratio) in the Bay of Bengal using isotopic composition of suspended particulate organic carbon and nitrogen, Deep-Sea Res., Part I, in press.
- Shetye, S. R., Shenoi, S.S.C., Gouveia, A. D., Michael, G.S., Sundar, D. and Nampoothiri, G. 1991. Wind driven coastal upwelling along the western boundary of the Bay of Bengal during the southwest monsoon. *Cont. Shelf Res.* **11**, 1397-1408.
- Shetye, S. R., Gouveia, A.D., Shenoi, S.S.C., Sundar, D. Michael, G.S. and Nampoothid, G.,1993. The western boundary current of the seasonal subtropical gyre in the Bay of Bengal. *J. Geophys. Res.***98**, 945-954.
- Shetye, S. R., Gouveia, A. D., Shankar, D., Shenoi, S. S. C., Vinayachandran, P. N. and co-authors., 1996. Hydrography and circulation in the western Bay of Bengal during the northeast monsoon. *J. Geophys. Res.* **101**, 14011-14025.
- Smith, S. J., Pitcher, H., Wigley, T. M. L., 2001. Global and regional anthropogenic sulfur dioxide emissions. *Glob. Planet. Change.* **29**, 99-119.
- Subrahmanyam, B., Murty, V.S.N., & Heffner, D. (2011), Sea surface salinity variability in the tropical Indian Ocean, *Remote Sens. Environ.*, **115**, 944-956.
- Suzuki, R. and Ishimaru, T.,1990. An improved method for the determination of phytoplankton chlorophyll using N,N-dimethylformamide. *J. Oceanogr.* **46**, 190-194.
- Tsunogai, S., Watanabe, S. and Sato, T., 1999. Is there a “continental shelf pump” for the absorption of atmospheric CO<sub>2</sub>?. *Tellus B.* **51**, 701-712.
- UNESCO, 1979. Discharge of Selected Rivers of the World. UNESCO, Paris.
- Varkey, M. J., Murthy, V. S. N. and Suryanarayana, A., 1996. Physical Oceanography of the Bay of Bengal and Andaman Sea. *Oceanogr. Marine Biol.: an Annual Rev.* (eds). A.D. Ansell, R.N. Gibson and Margaret Barnes, **34**, 1-70.

- Wanninkhof, R., 2014. Relationship between wind speed and gas exchange over the ocean revisited. *Limnol. Oceanogr. Methods*, doi:10.4319/lom.2014.12.351.
- Zhai, W.D., Dai, M., Cai, W.J., Wang, Y., and Hong, H. 2005. The partial pressure of carbon dioxide and air-sea fluxes in the northern South China Sea in spring, summer and autumn. *Mar. Chem.*, 96, 87-97.
- Zhai, W.D., Dai, M.H., Chen, B.S., Guo, X.H., Li, Q., Shang, S.L., Zhang, C.Y., Cai, W.J., and Wang, D.X. 2013. Seasonal variations of sea-air CO<sub>2</sub> fluxes in the largest tropical marginal sea (South China Sea) based on multiple-year underway measurements. *Biogeosciences*, 10, 7775-7791.
- Zhang, J. and Reid, J. S., 2010. A decadal regional and global trend analysis of the aerosol optical depth using a data-assimilation grade over-water MODIS and Level 2 MISR aerosol products. *Atmos. Chem. Phys.* **10**, 10949-10963.

## Legend to figures

- Figure 1:** Study area showing the locations of the time-series stations and ADCP measurements at off Visakhapatnam, in the coastal BoB. The Indian rivers network is shown in the inset.
- Figure 2:** Monthly variations in temperature, salinity and chlorophyll-a ( $\text{mg m}^{-3}$ ) during 2015 in the coastal BoB for the (left panel) inshore region ( $<15$  km distance from the coast) and offshore region ( $>15$  km distance from the coast).
- Figure 3:** Depth–time sections of 36 hour low-pass filtered and 5 day averaged (a) zonal current speed ( $\text{cm s}^{-1}$ ), (b) meridional current speed ( $\text{cm s}^{-1}$ ) and (c) depth integrated zonal and meridional volume transport per unit distance ( $\text{m}^2\text{s}^{-1}$ ) in the 20-180 m layer during March 2015 – February 2016.
- Figure 4:** Variations of monthly mean HYCOM simulated Sea Surface Height (SSH, colour shading) and circulation (current vectors) in the western BoB encompassing the study area for (a) February 2015, (b) May 2015, (c) August 2015 and (d) November 2015. For clarity, alternate current vectors with two grid points skipping are presented. The magnitude of current vector is marked in each figure. Colour code for SSH (m) is provided on the right side. Abscissa (Ordinate) represents the longitude (latitude). The inshore region (offshore region) locations are represented by red star (green dot). The Blue square represents the coastal mooring location for current observations.
- Figure 5:** Same as in Figure 4, but for weekly mean HYCOM simulated Sea Surface Height (SSH, colour shading) and circulation (current vectors) in the western BoB encompassing the study area for (a) 1<sup>st</sup> week of June 2015, (b) 3<sup>rd</sup> week of June 2015, (c) 1<sup>st</sup> week of July 2015 and (d) 3<sup>rd</sup> week of July 2015.
- Figure 6:** Monthly variations in DIC ( $\mu\text{M}$ ), pH (at *insitu* temperature),  $\text{pCO}_2$  ( $\mu\text{atm}$ ), calcite and aragonite saturation during 2015 in the coastal BoB for the inshore region (left panel) and offshore region (right panel).
- Figure 7:** Relationships of salinity, temperature and Chl-a with DIC. Maintain uniform temperature scale in the first top left corner figure.
- Figure 8:** Relationship of salinity with a) DIC ( $\mu\text{M}$ ) and b) computed TA ( $\mu\text{M}$ ) in the coastal (closed circles) and open sea region (open circles). The mixing line between freshwater and sea water end member (black) and linear regression line (Red line) were also plotted.
- Figure 9:** Monthly variations in the controlling factors – biological effect (green), mixing effect (blue), thermal effect (red) and flux effect (yellow) – of  $\text{pCO}_2$  in the coastal BoB for the (left panel) inshore region and (right panel) offshore region.

**Figure 1:** Study area showing the locations of the time-series stations and ADCP measurements at off Visakhapatnam, in the coastal BoB. The Indian rivers network is shown in the inset.

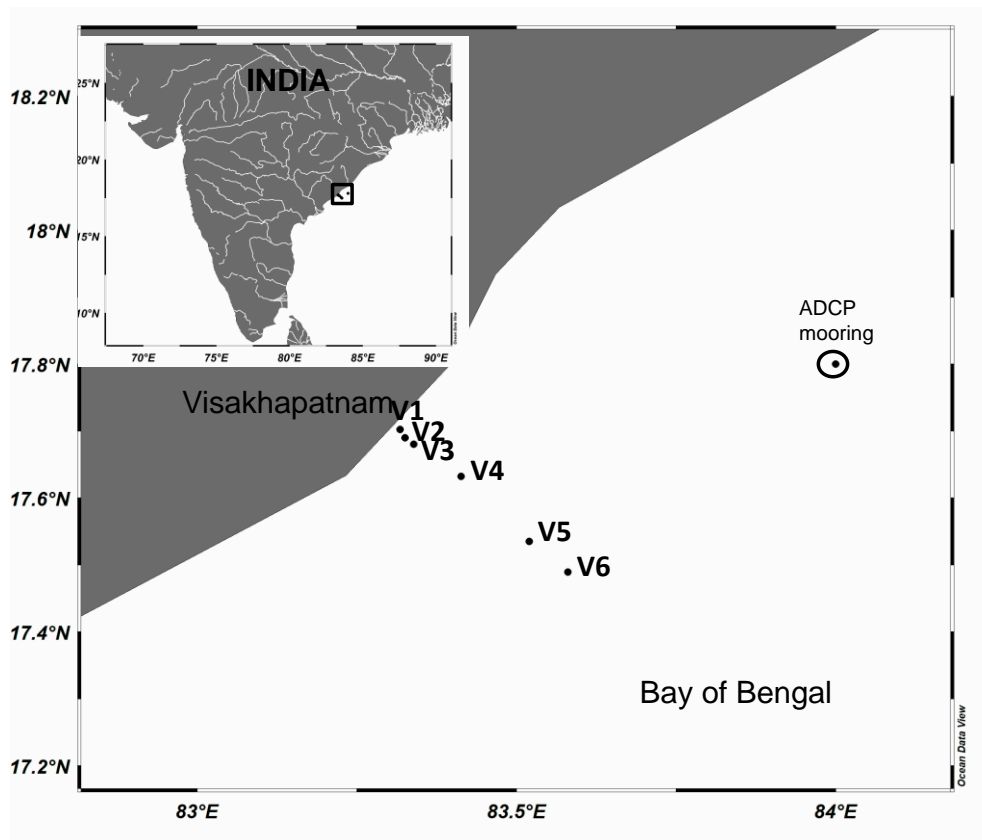


**Figure 2:** Monthly variations in temperature, salinity and chlorophyll-a ( $\text{mg m}^{-3}$ ) during 2015 in the coastal BoB for the (left panel) inshore region ( $<15$  km distance from the coast) and offshore region ( $>15$  km distance from the coast).

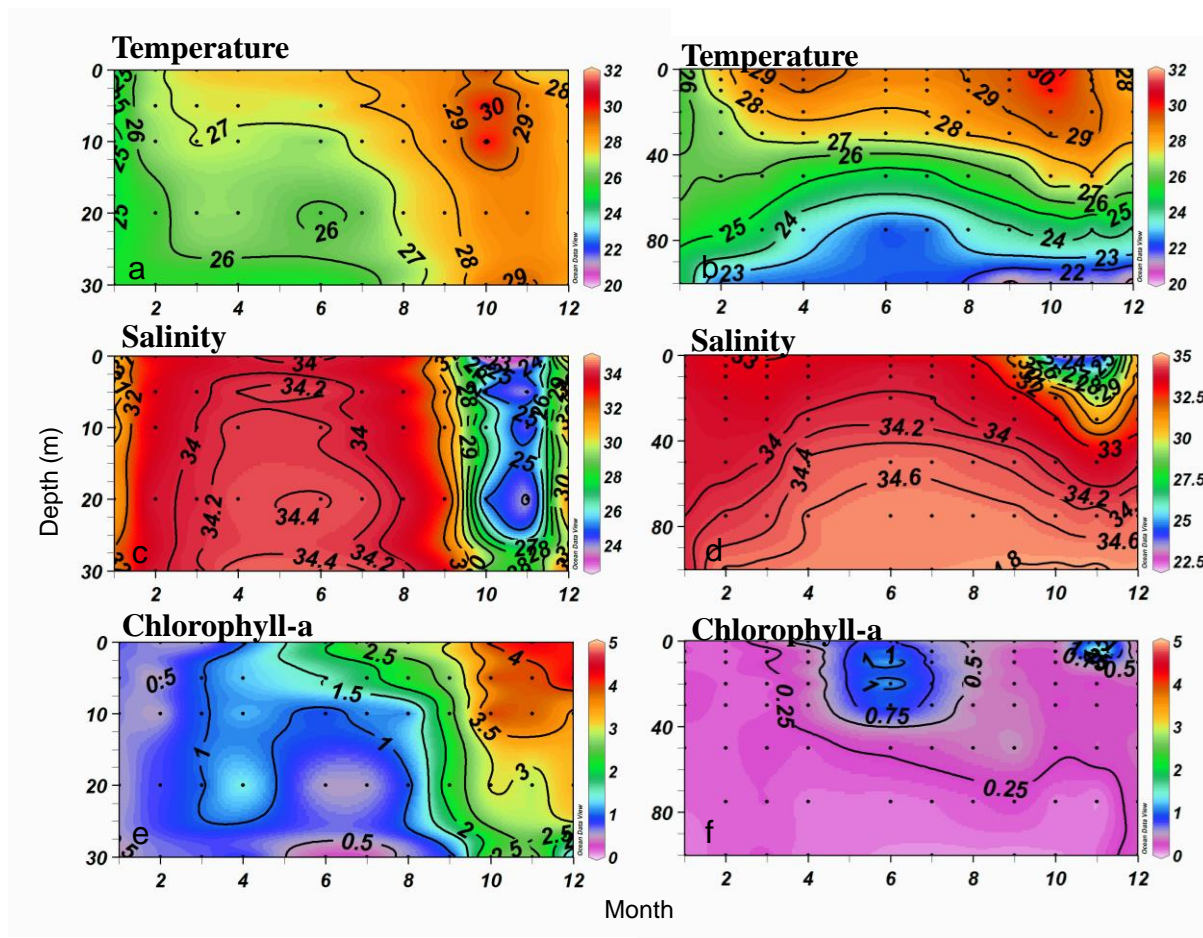


**Figure 3:** Depth–time sections of 36 hour low-pass filtered and 5 day averaged (a) zonal current speed ( $\text{cm s}^{-1}$ ), (b) meridional current speed ( $\text{cm s}^{-1}$ ) and (c) depth integrated zonal and meridional volume transport per unit distance ( $\text{m}^2\text{s}^{-1}$ ) in the 20-180 m layer during March 2015 – February 2016.

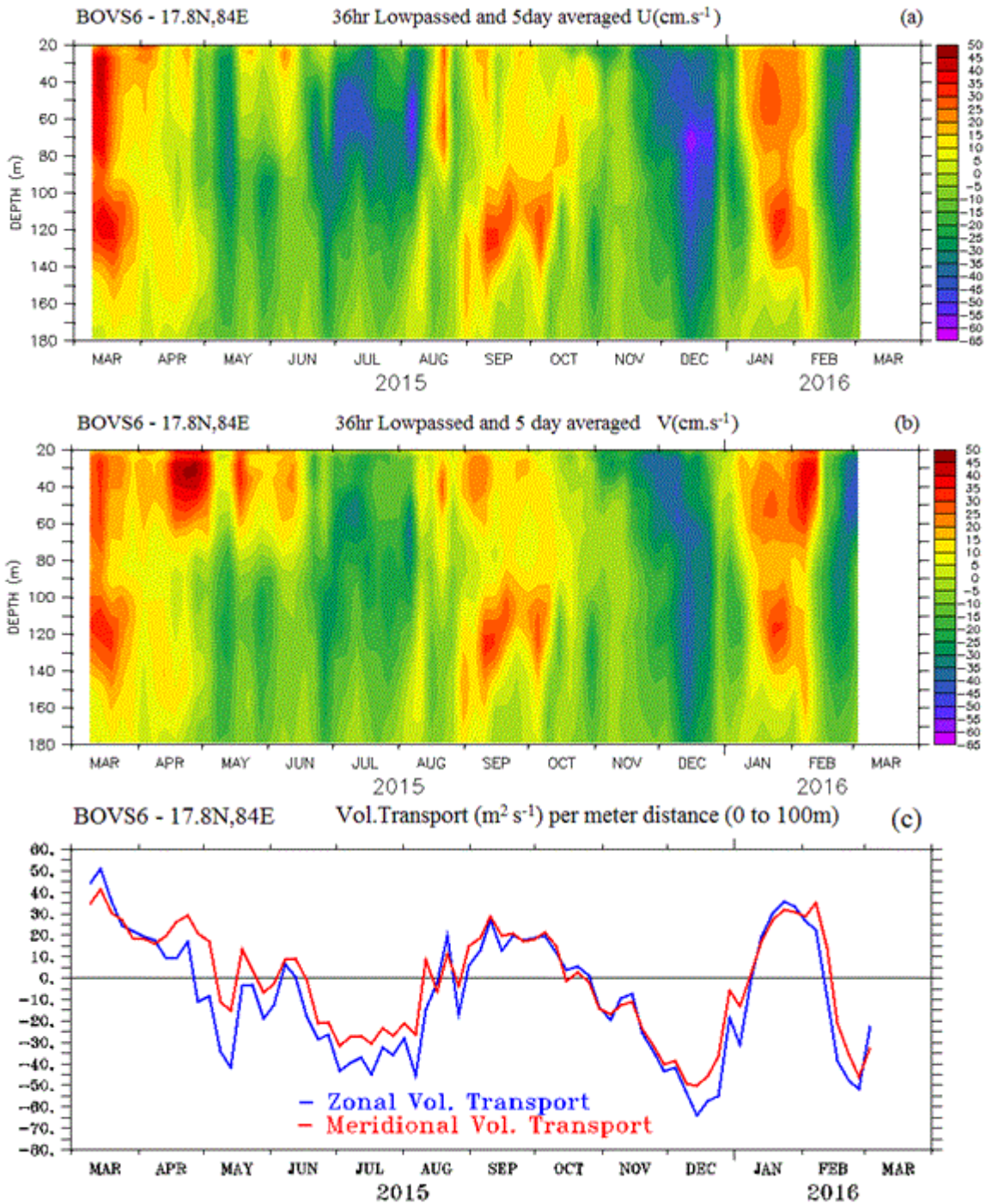




**Figure 4:** Variations of monthly mean HYCOM simulated Sea Surface Height (SSH, colour shading) and circulation (current vectors) in the western BoB encompassing the study area for (a) February 2015, (b) May 2015, (c) August 2015 and (d) November 2015. For clarity, alternate current vectors with two grid points skipping are presented. The magnitude of current vector is marked in each figure. Colour code for SSH (m) is provided on the right side. Abscissa (Ordinate) represents the longitude (latitude). The inshore region (offshore region) locations are represented by red star (green dot). The blue squares represents the coastal mooring location for current observations.

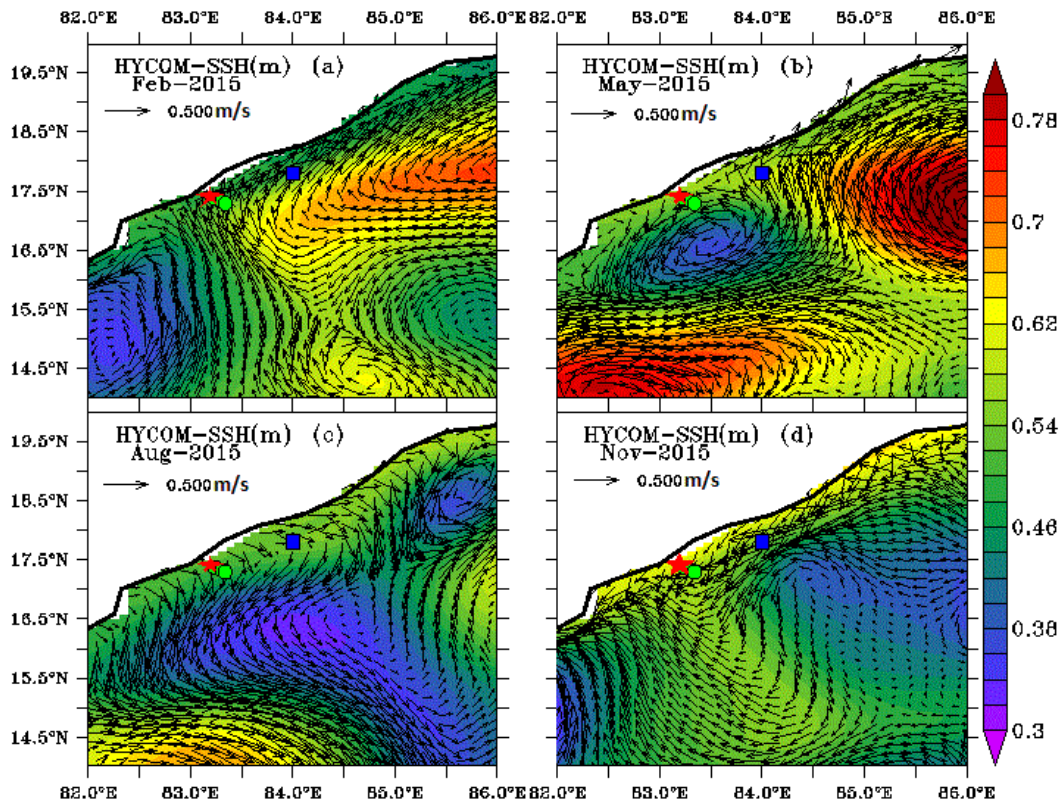


**Figure 5:** Same as in Figure 4, but for weekly mean HYCOM simulated Sea Surface Height (SSH, colour shading) and circulation (current vectors) in the western BoB encompassing the study area for (a) 1<sup>st</sup> week of June 2015, (b) 3<sup>rd</sup> week of June 2015, (c) 1<sup>st</sup> week of July 2015 and (d) 3<sup>rd</sup> week of July 2015.

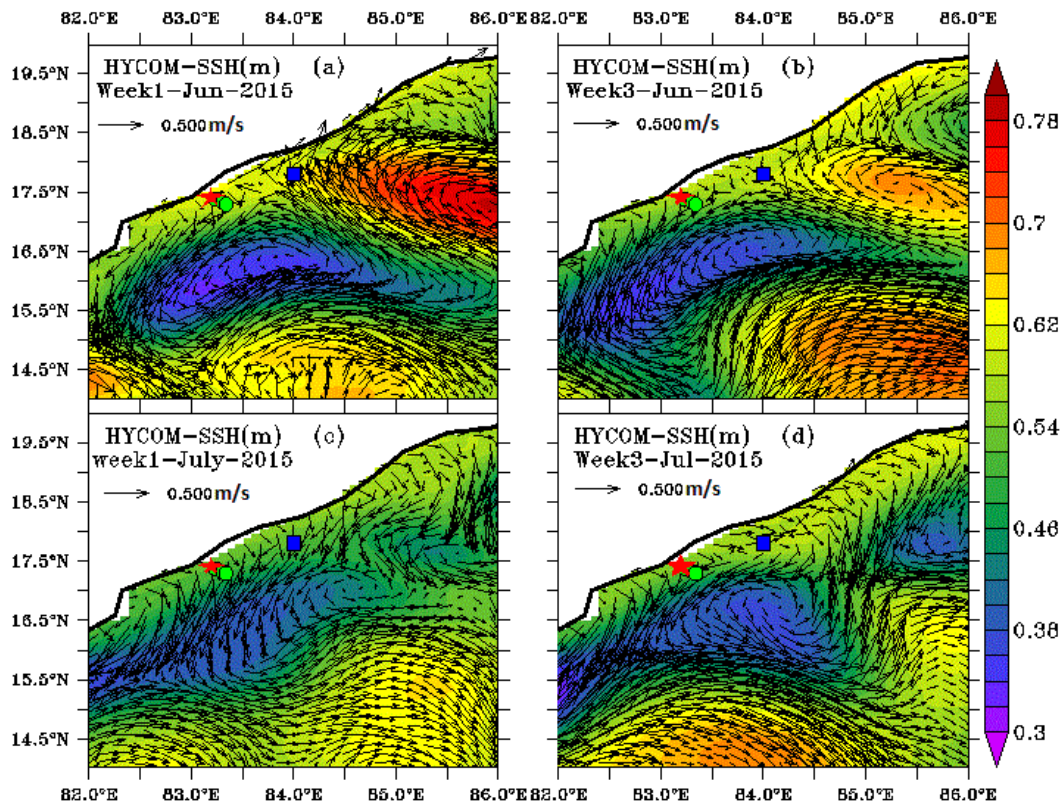


**Figure 6:** Monthly variations in DIC, pH, pCO<sub>2</sub>, calcite and aragonite saturation during 2015 in the coastal BoB for the (left panel) inshore region and (right panel) offshore region.

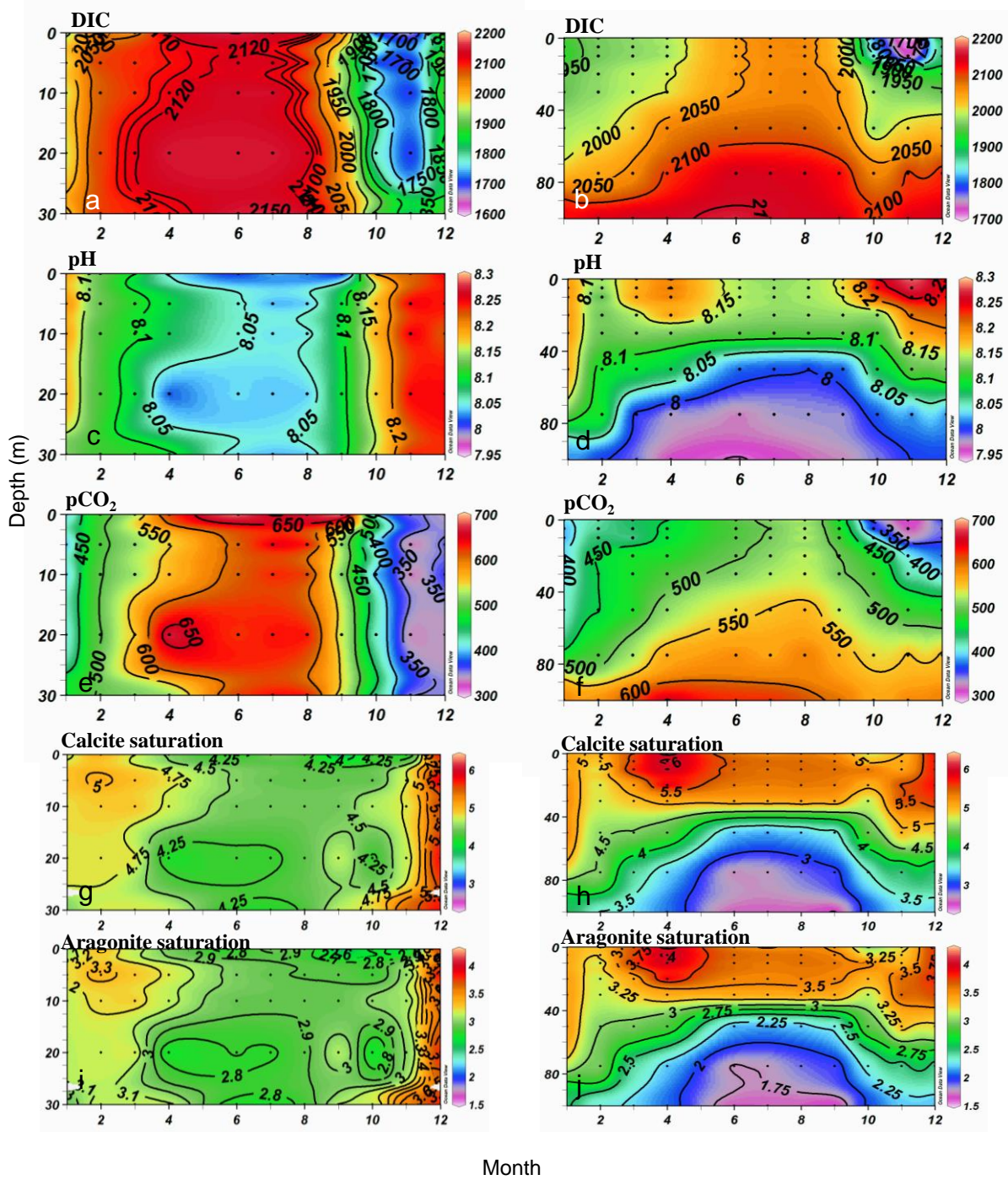


**Figure 7:** Relationships of salinity, temperature and Chl-a with DIC, pH and pCO<sub>2</sub> in the inshore (closed circles) and offshore (open circles) in the coastal BoB.

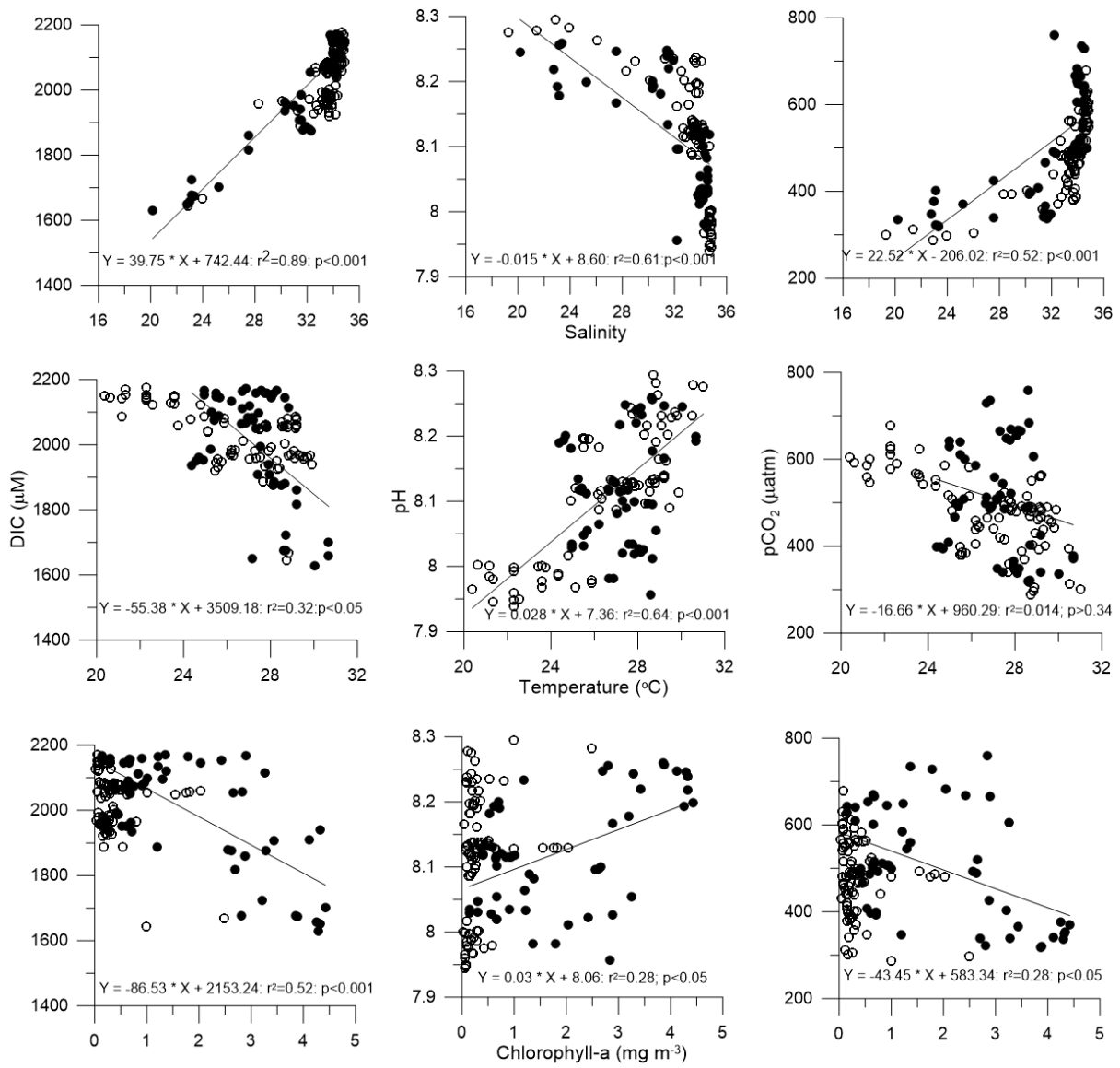


**Figure 8:** Relationship of salinity with a) DIC and b) computed TA in the coastal (closed circles) and open sea region (open circles). The mixing line between freshwater and sea water end member (black) and linear regression line (Red line) were also plotted.

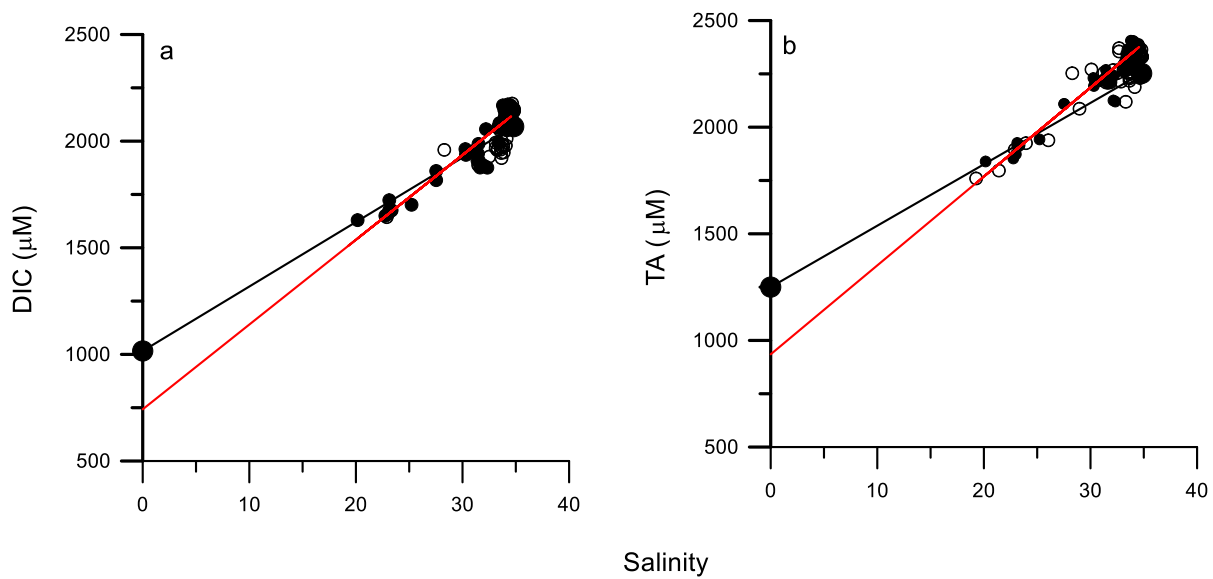


**Figure 9:** Monthly variations in the controlling factors – biological effect (green), mixing effect (blue), thermal effect (red) and flux effect (yellow) – of pCO<sub>2</sub> in the coastal BoB for the (left panel) inshore region and (right panel) offshore region.

